Distinguishing Potential Organic Biosignatures on Ocean Worlds from Abiotic Geochemical Products using Thermodynamic Calculations

Jordyn A. Robare[1], Everett L. Shock[1,2]

[1]School of Molecular Sciences and [2]School of Earth & Space Exploration, Arizona State University, Tempe, AZ 85357, USA

1. INTRODUCTION

Organic compounds have been detected all over the solar system – from meteorites (Burton et al., 2018; Cronin, 1989; Cronin and Pizzarello, 1983; Elsila et al., 2016; Epstein et al., 1987; Koga et al., 2017; Martins et al., 2008), comets (Mumma and Charnley, 2011), asteroids (De Sanctis et al., 2017; Nguyen et al., 2024), other planets (Freissinet et al., 2015), and icy moons (Postberg et al., 2008; Waite et al., 2009). In all these cases, the presence of organic molecules is not evidence of life since organic molecules can form abiotically, even on Earth (McDermott et al., 2015). Nevertheless, mass spectrometers are sent across the solar system to detect organic matter in the search for biosignatures. Doing so requires that we have a clear conception of how to identify a true biosignature. Thus far, there is no consensus method for classifying organic material as biotically sourced or abiotically sourced, and some current ideas are discussed below. As an example, monomeric and oligomeric organic compounds were assigned a medium to high confidence as a biosignature on NASA's Ladder of Life Detection (Neveu et al., 2018), while noting that there are sometimes abiotic synthesis pathways. With such uncertainty regarding the origin of organic compounds, there is a need for a process for sorting organic molecules into biotic and abiotic categories, which will be specific to each environment. The purpose of this study is to create a tool for discerning potential biosignatures using reaction thermodynamics.

Results from experiments on biotically and abiotically sourced organic molecules are used in proposed biosignature classification methods. One Enceladus analogue study compared how ratios of abiotically sourced amino and fatty acids and biologically selected ratios of amino and fatty acids were preserved after impact ionization of ice grains (Klenner et al., 2020). The results demonstrated that input ratios were conserved, thus allowing the discrimination of abiotic and biotic signatures. A limitation with this technique is that the interpretation of the source of the organics relies on what we know about biology on Earth. Another intriguing idea for biosignature classification is that of assembly theory (Marshall et al., 2021), which poses that only biotically sourced organic material can reach a certain level of complexity, and that complexity can be quantified. Assembly theory provides a lower threshold for molecular complexity based on life as we know it but does not address the thermodynamic potential for a molecule to be produced in its environment. In this study, we explore how the geochemical context of an organic molecule is crucial for interpretations of its synthetic origins. One way to investigate the origin of such compounds is by doing thermodynamic calculations for formation reactions from environmental precursors. Using thermodynamic calculations paired with other

classification methods may increase confidence in our ability to distinguish abiotic chemical signatures from biosignatures.

Life as we know it uses the same set of elements to build biomolecules. The bulk of biomass is comprised of carbon, hydrogen, nitrogen, oxygen, phosphorus, and sulfur, sometimes referred to as the CHNOPS elements. These elements, along with an energy source, are criteria that we can imagine extraterrestrial life requiring. Chemotrophs are organisms that capture energy without sunlight, using chemical disequilibria alone to fuel biochemical reactions. On ocean worlds such as Enceladus, the search for life would occur under the icy shell, in the subsurface ocean, where the sun does not reach. There, chemical disequilibria must provide energy for microorganisms. From CHNOPS-containing precursor molecules, we can evaluate the potential for organic synthesis via chemotrophy under the ice shell. We can investigate the thermodynamics of organic synthesis using CHNOPS species in the plume gas as reactants by calculating reaction affinities. Affinity is a measure of how far from equilibrium a reaction is. If a reaction has a positive affinity, it is thermodynamically favorable. If it has a negative affinity, the reaction is unfavorable but is favorable in the reverse direction. While catabolic, energy-releasing reactions may not be directly coupled to anabolic, biosynthesis reactions, the overall process must be energetically favorable. An intermediate step familiar from life on Earth is the storage of energy in adenosine triphosphate, commonly referred to as ATP. Despite intermediate reactions occurring in microbial metabolism linked by ATP, the overall reactions are sufficient for understanding the total change in energy, since this is a path-independent variable.

To quantify the affinity for a compound's synthesis, a decision must be made regarding the reactants. Perhaps there is a limited number of options to choose from for a given environment. If there is only one source of carbon, it may be the source for any coexisting organics. This decision becomes complicated when there are several options for reactants, and it is prudent to consider them all. While comparing reaction affinities for organic synthesis from different reactants, it is possible that the interpretation of their origin changes. If we do not test all options, we may incorrectly believe something is a potential biosignature. There is not a one-size-fits-all for biosignatures and the geochemical context should always be considered. The method presented here provides a new framework for interpreting the presence of organic molecules that may in the future be detected on ocean worlds. Any such method for interpreting biosignatures should be used in conjunction with other biosignature classification frameworks. Especially in the absence of authentic examples of biosignatures beyond Earth, many lines of evidence should be gathered and tested. Given the existence of necessary data, Saturn's moon Enceladus is used as an example of this general method.

2. METHODS

The Ion and Neutral Mass Spectrometer (INMS) and Cosmic Dust Analyzer (CDA) aboard the Cassini spacecraft detected several compounds in the plumes erupting from the cracks in the icy shell on Enceladus, often referred to as *tiger stripes* (Khawaja et al.,

2019; Postberg et al., 2023; Waite et al., 2009, 2017). Among the collected data, there was evidence for each of the CHNOPS elements. Recent analyses of Cassini's INMS data by Peter et al. (2023) include a statistically rigorous approach based on information theory in which previously unidentified species were brought forth as likely components of the plume gas and the confidence of each species was noted. Values from Peter et al., (2023), with constrained errors and statistical probabilities over 70%, were selected for the present study. The minimum and maximum volume mixing ratios (VMRs) – representing a percentage of the plume gas – of each species used in this study are displayed in Table 1. The values for several of these species are supported by evidence from Cassini's Ultraviolet Imaging Spectrograph (UVIS) (Hansen at el., 2020), including CO, NH_3 and CO_2. Peter et al. (2023) did not offer a new analysis of the abundance of H_2, citing its in-depth investigation by Waite et al. (2017), which was also adopted in this study. H_2S was not confidently constrained by Peter et al. (2023), with a value of <0.003% of the plume and a probability of 37%. Therefore, we adopted the value from Waite et al. (2009) – 0.0021% ± 0.001%, while acknowledging that this species is considered highly ambiguous (Magee & Waite, 2017). These numbers are in relative agreement and are used to calculate hypothetical affinities, so we accepted this uncertainty. Additionally, since sulfur is a minor component in most biomolecules, changes in this value are unlikely to strongly affect affinity results. To maintain consistency in this study, we are only using abundances determined by extrapolating data collected from INMS.

Table 1. Volume-mixing ratios of detected species adopted in this study

species	minimum %	maximum %	reference
H_2O	95.6	96.2	Peter et al. (2023)
CO_2	0.41	0.49	Peter et al. (2023)
CO	0.65	0.79	Peter et al. (2023)
CH_4	0.09	0.13	Peter et al. (2023)
H_2	0.4	1.4	Waite et al. (2017)
NH_3	1.7	1.9	Peter et al. (2023)
HCN	0.13	0.09	Peter et al. (2023)
C_2H_2	0.018	0.028	Peter et al. (2023)
C_3H_6	0.002	0.006	Peter et al. (2023)
C_2H_6	0.003	0.023	Peter et al. (2023)
H_2S	0.0011	0.0031	Waite et al. (2009)

Minimum and maximum volume-mixing-ratios as percentage of the plume gas. Minimum and maximum values are given as the lower and upper bounds of the mean values using their standard errors.

Using the ranges of CO_2 detected by the INMS, observed temperatures of the tiger stripes (Goguen et al., 2012), and saturation vapor pressures of ice at relevant temperatures (Haynes, 2014), the log activities of CO_2 in the subsurface ocean were constrained to a range of -5.9 and -2.8 by Glein et al. (2020). In the present study, we use the same method to constrain the aqueous activities of several species quantified by INMS. The CO_2 activity in the ocean was further constrained by Glein et al. (2020) using

CDA data for salt-rich ice grains measured in the plume. However, aqueous activities of other molecules could not be constrained in this manner, so the wider range of CO_2 abundance determined solely by INMS was adopted in this study. This maintains consistency in calculations among the other detected species. The method for determining aqueous activities from INMS data is briefly described here, as a series of steps starting from the plume gas and back-calculating activities in the ocean. This process is depicted schematically in Fig 1A.

The abundance of each species detected in the plume gas was assumed to remain constant once escaping the tiger stripes in the ice shell on Enceladus (Glein et al., 2015, 2020). Under this assumption, each frozen droplet contained a conserved ratio of species including water as it traveled up the plume and into the INMS. Based on this assumption, the VMR at Cassini was equal to the VMR immediately above the ice shell. However, within the fissures in the ice shell, water likely condensed onto the ice as it moved away from the ocean, enriching the plume gas in solutes relative to the underlying ocean. Removal of water from the plume can be modeled by comparing vapor saturation pressures of water above ice at the temperature of the ocean and at the temperatures measured at the top of the tiger stripes. Traversing Baghdad Sulcus, one of the major tiger stripes on the moon's south pole, Cassini's Visual Infrared Mapping Spectrometer (VIMS) measured temperatures of 177-217 K (Goguen et al., 2013). This range was assumed to represent the temperatures of the consortia of fissures from which solutes escaped. Glein et al. (2015) showed that experimentally determined steam densities (Haynes, 2014) at these temperatures and the 273.15 K subsurface ocean can be fit to obtain

$$\log \frac{\rho_{steam,tiger}}{\rho_{steam,ocean}} = 9.429 - \frac{2574}{T_{tiger}} \quad , \qquad (1)$$

where $\rho_{steam,location}$ represents the density of steam at the given location according to its temperature. The resulting density ratio can be used to calculate volume mixing ratios, $VMR_{i,location}$, of species *i* in the gas phase immediately above the ocean-gas interface or immediately above the tiger stripes using

$$VMR_{i,ocean} = \frac{\rho_{steam,tiger} \times VMR_{i,tiger}}{\rho_{steam,ocean}} \quad . \qquad (2)$$

It was assumed that the VMR of each species is the same right above the ocean as in the ocean as the droplets of ocean water would flash-freeze, preventing species from entering or exiting. Supporting evidence comes from recent experiments by Neveu et al. (2024), who showed that fractional abundances of amino and fatty acids recovered after evacuating and condensing water vapor are largely reflective of their fractional abundance in the aqueous source, even regardless of charge. VMRs of each species right above the ocean can be converted into molality *m* of species *i* using

$$m_i = \frac{VMR_{i,ocean} \times 1000}{M_{H_2O}} \quad , \qquad (3)$$

where M_{H2O} stands for the molar mass of water. Activities of neutral solutes can be assumed to approximately equal molality since solutions can be treated as ideal if all interactions among solutes are assumed to be identical (Anderson, 2015), and the ocean is not a concentrated brine (Postberg et al., 2009). The activities of solutes in the ocean are calculated by reference to the temperature of the tiger stripes, which has a constrained range of 40 Kelvin. Depending on abundances detected for each species and the temperature at which they escaped from the tiger-stripe fissures, log activities in the ocean for the compounds other than H_2O listed in Table 1 range from -8.33 to -2.42 as shown in Fig 1B. Affinity results using these activities are therefore also presented as functions of this temperature range to capture the variability invoked by the range of tiger-stripe temperatures. Note that while results are displayed as functions of the tiger-stripe temperatures, all affinity calculations were done at 273.15 K, the presumed temperature of the ocean at the ice-water interface.

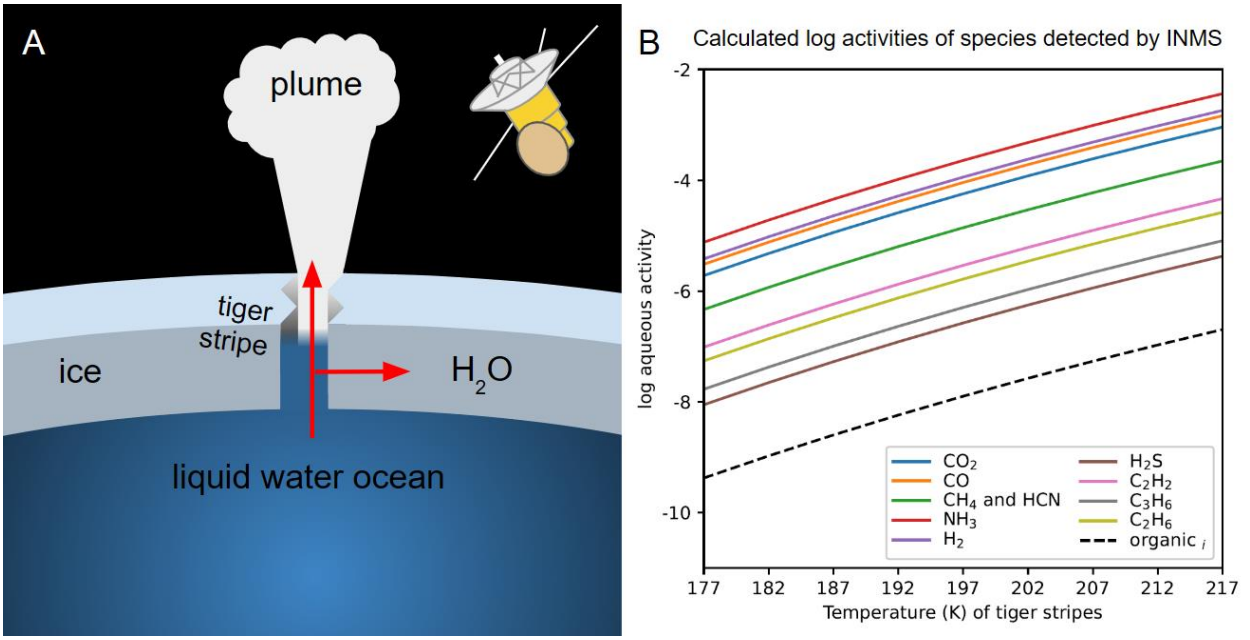

Figure 1. (A) Schematic of assumptions concerning the outer layers of Enceladus, where H_2 (and other solutes) and H_2O erupt from the subsurface ocean as a plume of gas. As solutes and H_2O vaporize and travel through the tiger stripes, H_2O condenses onto the surrounding ice shell as it travels outward, enriching the plume in solutes. Once out of the ice shell conduit, the ratio of solutes to H_2O remains the same as the gases expand into the vacuum of space and are detected by Cassini's INMS. (B) Calculated log aqueous activities (at 273.15 K) of constrained species, resulting from the process illustrated in the left panel using data from Table 1, are displayed as functions of tiger-stripe temperatures. The dashed curve represents a hypothetical organic molecule detected at 1 ppm in the plume gas and then converted into log aqueous activity.

To demonstrate the importance of considering all options for potential metabolic reactions, synthesis reactions were written from detected precursor species to neutral aqueous organic molecules containing carbon (C), hydrogen (H), nitrogen (N), oxygen (O), and/or sulfur (S) in the pyCHNOSZ database, a python wrapper (Boyer, 2021) for R package CHNOSZ (Dick, 2019). Thermodynamic data for all reaction species are

contained in this database, compiled from original sources (Amend & Helgeson, 1997; Canovas & Shock, 2016; Dale et al., 1997; Dick et al., 2013; Hawrylak et al., 2006; Kitadai, 2014; LaRowe & Amend, 2016, 2019; LaRowe & Dick, 2012; LaRowe & Helgeson, 2006; Plyasunov & Shock, 2001; Schulte, 2010; Schulte & Rogers, 2004; Schulte & Shock, 1993; Shock, 1993; 1995; Shock & Helgeson, 1990; Shock & Koretsky, 1993; Shock & McKinnon, 1993). By doing these calculations, we inclusively simulate the detection of small and large organics in the plume gas despite INMS's upper mass limit of 99 amu (Waite et al., 2004) and explore the implications of detecting these hypothetical organic molecules for future missions. In fact, some of the organics considered in this study were detected in low abundances by INMS (Waite et al., 2009) and with some ambiguity by CDA due to its low mass resolution and ionization method (Khawaja et al., 2019). Reactions were balanced with H_2O and H_2. Reactions to form organic compounds involving nitrogen and/or sulfur were balanced with a nitrogen source and/or H_2S, respectively. Nitrogen sources included NH_3 and HCN. Affinities for reactions involving all combinations of carbon and nitrogen sources were evaluated. Using 273.15 K for the temperature of the ocean (Glein et al., 2015), equilibrium constants for synthesis reactions, K_r, were calculated in pyCHNOSZ, using a pressure of 1 bar. One estimated maximum pressure at the deepest part of the ocean is 74 bars (Glein et al., 2018) and the change in activities and affinities from 1 to 74 bars is negligible. The activity product, Q_r, was defined for each reaction as the product of all activities, a, of each species i in the reaction raised to its stoichiometric reaction coefficient, ν_i, using

$$Qr = \prod a_i^{\nu_i} \quad . \tag{4}$$

To represent a reasonable detection limit for mass spectrometers sent on future missions, a conservative 1 ppm was used as the abundance of organic molecules in the gas phase. This, along with the VMR of each species in Table 1, were converted into aqueous activities using Eq 1-3. The aqueous log activities of a hypothetically detected molecule in the ocean of Enceladus is shown in Fig. 1B. Note that for reactants, ν is negative, and for products, ν is positive. Using a ratio of the equilibrium constant, K_r, and reaction quotient, Q_r, for each reaction, the affinity, A_r, in joules per mole of reaction, was calculated using

$$A_r = RT \ln \frac{K_r}{Q_r} \tag{5}$$

where R stands for the ideal gas constant and T indicates temperature in Kelvin.

3. RESULTS

To explain the affinity results reported in this study, two aqueous molecules – phenanthrene and alanine – were chosen as examples to represent hypothetical organic molecules detected at 1 ppm in the plume. These compounds were chosen to demonstrate the effects of molecular mass on affinities. The same calculations were undertaken for an additional 211 organic molecules (see supplementary information). Balanced formation reactions from each carbon source are displayed in Tables 2 and 3.

The affinities for each of these reactions across the range of tiger-stripe temperatures were calculated. The average affinities at 273.15 K using the abundances calculated for outgassing at the median temperature (197 K) in the range for the tiger stripes are given in the tables, along with the error associated with these values caused by uncertainties in the VMR ranges for reactants (Waite et al., 2009, 2017; Peter et al., 2023). For simplicity, only NH_3 was considered as a source of nitrogen in these examples.

The average oxidation state of carbon, $\bar{Z}_C$, of the carbon sources and the organic molecules were calculated using

$$\bar{Z}_C = \frac{Z - n_H + 2(n_O + n_S) + 3n_C}{n_C} \quad (6)$$

where Z is the overall charge of the molecule, and n_H, n_O, n_S, n_N, and n_C are the numbers of hydrogen, oxygen, sulfur, nitrogen, and carbon atoms in the molecule, respectively (see Dick & Shock, 2011). The effect of the full temperature range of the tiger stripes on these affinity calculations, owing to variations in the calculated activities of aqueous solutes involved in the reactions, is displayed in Figure 2.

Table 2. Phenanthrene synthesis reactions from each aqueous carbon source.

$\bar{Z}_C$	Reaction	$\bar{Z}_C$ phenanthrene: -0.71		Affinity (kJ/mol)	error (kJ/mol)
-4	14 CH_4	= $C_{14}H_{10}$ (phenanthrene)	+ 23 H_2	-1032.61	+48/-29
-3	7 C_2H_6	= $C_{14}H_{10}$ (phenanthrene)	+ 16 H_2	-547.66	+39/-39
-2	4.67 C_3H_6	= $C_{14}H_{10}$ (phenanthrene)	+ 9 H_2	-38.22	+21/-16
-1	7 C_2H_2	= $C_{14}H_{10}$ (phenanthrene)	+ 2 H_2	1075.38	+7/-6
+2	14 CO + 19 H_2	= $C_{14}H_{10}$ (phenanthrene)	+ 14 H_2O	1056.10	+22/-38
+2	14 HCN + 19 H_2	= $C_{14}H_{10}$ (phenanthrene)	+ 14 NH_3	1667.90	+15/-31
+4	14 CO_2 + 33 H_2	= $C_{14}H_{10}$ (phenanthrene)	+ 28 H_2O	598.18	+36/-64

Table 2. Example formation reactions were written from each carbon source to aqueous phenanthrene, balancing with H_2, H_2O, and NH_3 when HCN is the carbon source. $\bar{Z}_C$ of the product is given above the reactions, and $\bar{Z}_C$ of carbon sources are written to the left of each reaction. Using activities at the midpoint of the tiger-stripe temperature range (197 K) yields the affinities reported to the right of the reactions at 273.15 K, along with the errors evaluated from the minimum and maximum VMRs for reactants and products. The errors are asymmetric because converting from reaction products (Q_r) to affinities (A_r) involves taking a logarithm.

Table 3. Alanine synthesis reactions written from each aqueous carbon source.

$\bar{Z}_C$	Reaction	$\bar{Z}_C$ alanine: 0		Affinity (kJ/mol)	error (kJ/mol)
-4	3 CH_4 + 2 H_2O + NH_3	= $C_6H_8O_7$ (alanine)	+ 6 H_2	-267.90	+12/-8
-3	1.5 C_2H_6 + 2 H_2O + NH_3	= $C_6H_8O_7$ (alanine)	+ 4.5 H_2	-163.99	+10/-10
-2	1 C_3H_6 + 2 H_2O + NH_3	= $C_6H_8O_7$ (alanine)	+ 3 H_2	-54.82	+7/-5
-1	1.5 C_2H_2 + 2 H_2O + NH_3	= $C_6H_8O_7$ (alanine)	+ 1.5 H_2	183.81	+4/-2
+2	3 CO + 3 H_2 + NH_3	= $C_6H_8O_7$ (alanine)	+ H_2O	179.68	+4/-6
+2	3 HCN + 2 H_2O + 3 H_2	= $C_6H_8O_7$ (alanine)	+ NH_3	310.78	+2/-5
+4	3 CO_2 + 6 H_2 + NH_3	= $C_6H_8O_7$ (alanine)	+ 4 H_2O	81.55	+7/-12

Table 3. Example formation reactions were written from each carbon source and NH_3 to aqueous alanine, balancing with H_2, H_2O. $\bar{Z}_C$ of the product is given above the reactions, and $\bar{Z}_C$ of carbon sources are written to the left of each reaction. Using activities at the midpoint of the tiger-stripe temperature range (197 K) yields the affinities reported to the right of the reactions at 273.15 K, along with the errors evaluated from the minimum and maximum VMRs for reactants and products. The errors are asymmetric because converting from reaction products (Q_r) to affinities (A_r) involves taking a logarithm.

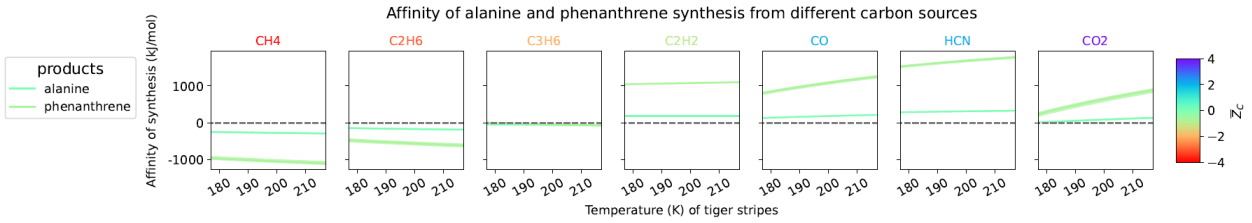

Figure 2. Results of affinity calculations (at 273.15K) from reactions forming aqueous phenanthrene and alanine from all possible carbon sources quantified in the plume gas, as listed in Tables 2 and 3, plotted as functions of the temperature range of the tiger stripes. Reactants are displayed in order of increasing $\bar{Z}_C$ and affinity curves are colored by the $\bar{Z}_C$ of their product.

Affinity results in Fig 2 are displayed by order of increasing $\bar{Z}_C$ of the reactants. We can see that, when using CH_4 as the carbon source, both aqueous products have negative affinities, meaning that their syntheses would require energy if synthesized from the reactions in Tables 2 and 3. Synthesis of phenanthrene, which has a formula of $C_{14}H_{10}$, requires more moles of each carbon source than does that of alanine, which has a formula of $C_3H_7NO_2$. This inflates the magnitude of the affinity results for phenanthrene, while the affinity of alanine remains closer to 0. Reactions from CH_4 to phenanthrene and alanine yield the most negative affinities compared to all carbon sources. Reactions using either C_2H_6 or C_3H_6 are also accompanied by negative affinities, although those for C_3H_6 are only slightly negative. The affinity results become positive when using carbon sources with $\bar{Z}_C$ above that of C_3H_6. Synthesis of phenanthrene from the remaining carbon sources would release energy if the reaction progressed from the starting activities calculated in this work. Note that calculations for reactions starting with C_2H_2, CO and HCN yield more positive affinities than those from CO_2.

Many factors contribute to the calculated affinity of each formation reaction. Including the examples above, we wrote reactions to form 213 organic compounds from each of the carbon sources and organized the resulting affinities into 23 groups as shown in the supplementary information. These include alkanes, alkenes, alkynes, alcohols, ketones, aldehydes, normal carboxylic acids, dicarboxylic acids, 2-hydroxyacids, amino acids, other acids, aromatic compounds, phenols, phenanthrenes, sugars, alkylamines, peptides, nucleobases, nucleosides, deoxyribonucleosides, thiols, sulfides, and other miscellaneous compounds. In the supplementary information, affinities for synthesis from CH_4 and NH_3 are shown in Fig S1, from C_2H_6 and NH_3 in Fig S2, from C_3H_6 and NH_3 in Fig S3, from C_2H_2 and NH_3 in Fig S4, from HCN and NH_3 in Fig S5, from CO and NH_3 in Fig S6 and from CO_2 and NH_3 in Fig S7.

For a more textured example of the multitude of affinities calculated in this study, the results for affinities of formation of all biogenic amino acids taken from the supplementary information are shown in Fig 3. In this analysis, HCN was used both as a carbon source and as a nitrogen source. Due to issues with stoichiometry, it cannot be used as both, as represented by the open frame in the figure. $\bar{Z}_C$ values for amino acids vary from +1 to -1 (Dick & Shock, 2021), resulting in the narrow portion of the color spectrum attained by these results. In most cases, the amino acid plotting closest to A_r = 0 is the smallest amino acid, glycine. The magnitude of affinity is greatest for the largest amino acids: phenylalanine, tryptophan and tyrosine. However, the sign of the affinity curves changes depending on the carbon source. As a result, the affinities for the largest amino acids are either more strongly negative, corresponding to a greater input of energy for synthesis, as in the case of CH_4, or more strongly positive as in the case of HCN.

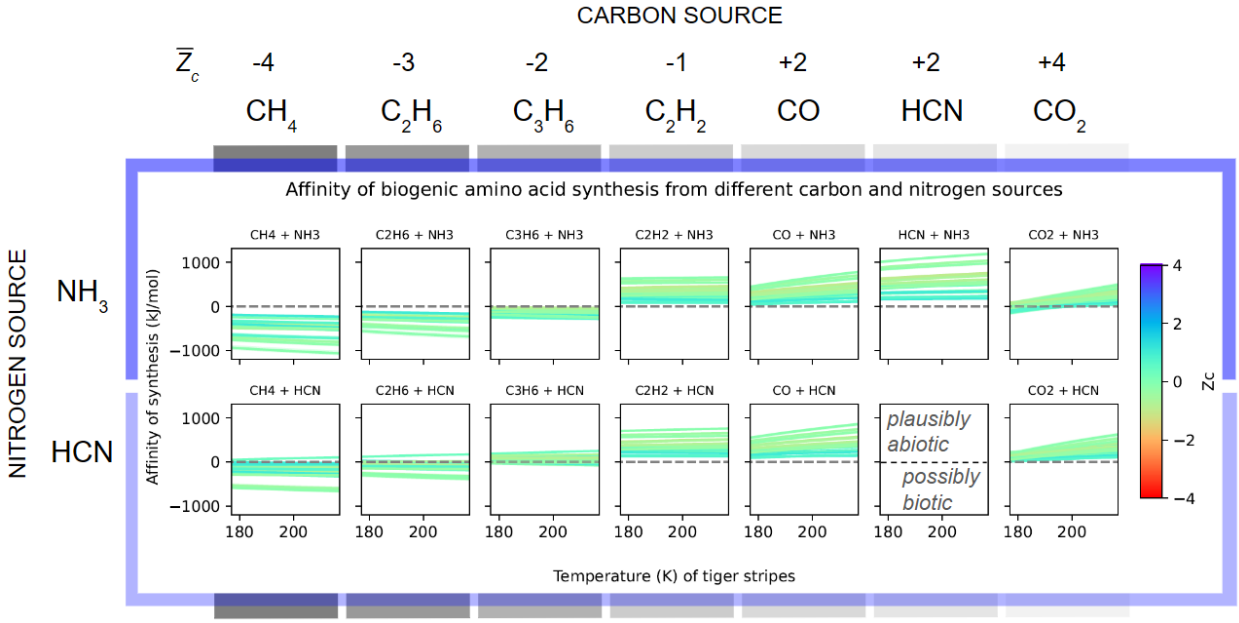

Figure 3. Comparison of different carbon and nitrogen sources on affinities of amino acid synthesis reactions at 273.15 K plotted against the tiger-stripe temperatures used to determine reactant and product activities in the ocean on Enceladus. Note that affinities are negative for synthesis from NH_3 and CH_4, C_2H_6, or C_3H_6, and positive for synthesis from C_2H_2, CO, and HCN. Results for synthesis from NH_3 and CO_2 are mixed. In general, affinities for corresponding amino acid synthesis reactions with HCN as the nitrogen source are more positive than those using NH_3.

When comparing results in Fig 3 between NH_3 and HCN as nitrogen sources, it becomes apparent that reactions involving HCN have slightly elevated reaction affinities. This arises from the relative instability of the HCN molecule compared to NH_3. The overall shapes of the curves are similar between nitrogen sources. On the other hand, the affinities are significantly more positive when using HCN as a carbon source than those from other carbon sources. For this reason and to reduce dimensionality for improved comprehension, the results shown subsequent to Fig 3 and in the supplementary information consider HCN only as a carbon source and NH_3 as the sole nitrogen source. Formation reactions, like those shown for phenanthrene and alanine in Tables 2 and 3,

were written from all carbon sources detected on Enceladus in resolvable quantities to all aqueous organic compounds in the pyCHNOSZ database, using NH_3, H_2S, H_2, and H_2O to balance. The position of the calculated affinities with respect to the equilibrium lines shown in the figures above can help us sort detected molecules into two categories: *plausibly abiotic* above $A = 0$ and *possibly biotic* below.

4. DISCUSSION

4.1 The example of Enceladus

Enceladus is a primary target in the search for life in our solar system (McKay et al., 2014; Sherwood Lollar et al., 2018). Plumes erupting through cracks in its exterior ice shell provide evidence for the chemical composition of the subsurface ocean, where the search for life is targeted. The INMS aboard Cassini had an upper mass limit of 99 amu (Waite et al., 2004). This limit precludes anything heavier than a heptane molecule, including most amino acids and all nucleobases, carbohydrates, and cell membrane lipids along with their degradation products. Therefore, even if these molecules did exist in the plume, INMS would not have detected them. The CDA, however, had a nominal upper mass limit of 200 amu, which could be expanded to 8,000 amu at the cost of a ten-fold decrease in resolution and sensitivity (Postberg et al., 2018). Nonspecific, high molecular mass signatures around 200-500 amu, 1,000 amu, and 1,700 amu indicated the existence of macromolecules on Enceladus, perhaps in the form of an organic layer above the ocean. For the purposes of this study, we narrow our calculations to organic compounds dissolved in the ocean. As these limitations on spacecraft instrumentation are surpassed, we may begin to identify and quantify complex organic molecules during our exploration of the solar system.

4.2 Organics in the solar system

The abundance of organic molecules already found in comets (Burton et al., 2018; Cronin, 1989; Cronin and Pizzarello, 1983; Elsila et al., 2016; Epstein et al., 1987; Koga et al., 2017; Martins et al., 2008) may suggest that their presence is ubiquitous in the solar system. These previously discovered organic molecules are not presumed to be of biological origin and are instead thought to be abiotic byproducts of processes in the solar nebula or parent-body processes including water-rock interactions. This implies that their synthesis was thermodynamically favorable in their original environment (Shock and Schulte, 1990), unless exogenous energy sources helped promote the reaction. Separating synthesis reactions by whether they are thermodynamically favorable or unfavorable with respect to their environment allows us to explore their potential sources. This categorization is particularly useful because of life's ability to link thermodynamically unfavorable biochemical reactions with more favorable energy-capturing reactions. Chemotrophic organisms fuel biosynthesis reactions using chemical energy acquired from their environment, while photosynthesizers use the energy from sunlight. We can see that plant matter is actually unstable based on how readily it reacts with the oxygen in our atmosphere during a forest fire. Quantifying the energy change during organic

synthesis can help us judge whether an organic molecule may have formed biotically or abiotically.

4.3 Exploring affinities from various carbon sources

However, we need to take care to not fall into the trap of an Earthly biological bias. On Earth, we may primarily think about CO_2 as a carbon source since it feeds the plant life around us. Several known carbon fixation pathways that use CO_2 on Earth are listed in Barge and Fournier (2024) along with their advantages and disadvantages within the context of Enceladus. In a study by Liu et al. (2024), the thermodynamic potential for organic synthesis from CO_2 was calculated as a function of pH, and hence, as a function of the abundance of reactants (Glein & Waite, 2020). We may build our biosignature categorizer around the assumption that CO_2 is the only possible carbon source on Enceladus, but there are other possible carbon sources that have been detected with high confidence including CH_4, CO, C_2H_6, C_3H_6, C_2H_2, and HCN (Peter et al., 2023). There is evidence that most of these can be used as energy sources by organisms on Earth (Ensign et al., 1992; Hahn et al., 2021; King et al., 2007; Rosner et al., 1997). Some of these carbon sources are less commonly considered and may be overlooked as metabolic options or even abiotic building blocks when investigating origins of organic compounds in our solar system. As revealed in this study, synthesis from some of these alternate carbons sources is substantially more favorable than from CO_2.

4.3.1 Thermodynamic properties

To explore how the choice of reactants affects reaction affinities, and therefore our interpretation of chemical signatures found on ocean worlds, we can examine the effect of each variable in the affinity calculation (Eqn 5). First, we can consider K_r, or the equilibrium constant for the reaction, which is calculated using

$$\Delta_r G° = -RT \ln K_r \quad (7)$$

where $\Delta_r G°$ represents the standard state Gibbs energy of a reaction. $\Delta_r G°$ is calculated using

$$\Delta_r G° = \sum \nu_i \times \Delta_f G°_i \quad (8)$$

where ν_i represents the stoichiometric reaction coefficient of species *i* in the reaction and $\Delta_f G°_i$ indicates the apparent standard Gibbs energy of formation of that species at any temperature and pressure. To compare the effects of the thermodynamic properties of each carbon source on affinity, $\Delta_f G°$ of each carbon source was calculated at 273.15 K using pyCHNOSZ (Dick, 2019; Boyer, 2021). The affinities of all reactions from each carbon source were averaged and plotted against $\Delta_f G°$ of each carbon source, as shown in Fig 4.

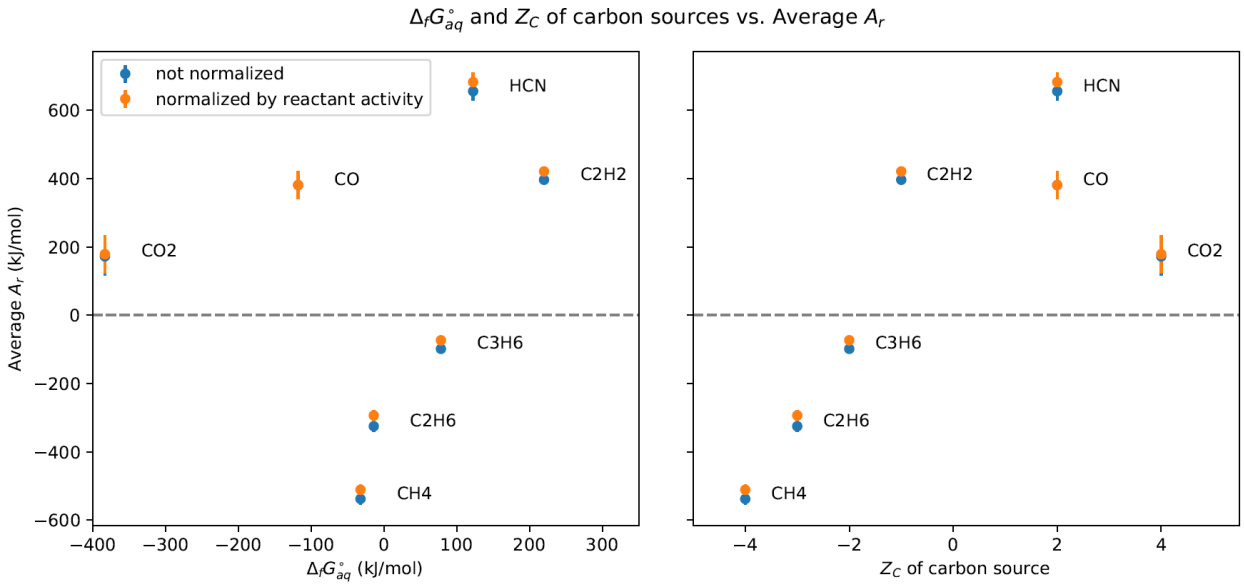

Figure 4. (left) For simplicity, only VMRs calculated as if they escaped the tiger stripes at the median temperature (197 K) were used to calculate the affinities in this figure. The reaction affinities from each carbon source were averaged and then plotted as a function of $\Delta_f G^\circ_i$ of the respective carbon source. Note that affinity calculations were performed at 273.15 K. Calculations done using reported VMRs are displayed in blue, while values set to the VMR of CO are displayed in orange. Standard deviations in affinities are plotted as vertical lines across points. A grey dashed line denotes an affinity of 0, or equilibrium. (right) The same affinity values are plotted against $\bar{Z}_c$ of each carbon source.

4.3.2 Carbon oxidation states and the redox environment

As seen in Fig 4, the $\Delta_f G^\circ_i$ values of carbon sources do not easily explain the calculated reaction affinities from those carbon sources. A somewhat clearer trend emerges when displaying these affinities as functions of the $\bar{Z}_C$ of each carbon source. Reactions from the carbon source with the lowest $\bar{Z}_C$ (CH_4 with a $\bar{Z}_C$ of -4) yield the lowest average affinities. Typically, as $\bar{Z}_C$ increases, so does the average reaction affinity. However, they peak before the most oxidized carbon source – CO_2. In a previous study, methanogenesis, that is the production of CH_4 from CO_2 and H_2, on Enceladus was calculated to have a positive affinity and could therefore be a plausible metabolism for microorganisms (Waite et al., 2017). We have reproduced this result (Fig S7, first panel, lowest curve) and show that, alternatively, CH_4 consumption to form organic molecules is not thermodynamically favorable (see also Fig S1). Consecutively, C_2H_6, and C_3H_6, with respective $\bar{Z}_C$ of -3, and -2, yield increasingly higher affinities, albeit still negative (see also Figs S2 and S3). This linear trajectory ends in an average positive affinity for reactions involving C_2H_2, which has a $\bar{Z}_C$ of -1 and was shown by Yanez et al. (2024) to be an exergonic metabolic option at Enceladus (see also Fig S4). The remaining carbon sources, CO, HCN, and CO_2, have $\bar{Z}_C$ of +2, +2, and +4, and also yield positive affinities (see also Figs S5-S7), with reactions involving HCN yielding the highest average affinities (see Fig 5). Overall, carbon sources with $\bar{Z}_C \geq -1$ yield positive reaction affinities. Additionally, plotting affinities as functions of the $\Delta_f G^\circ$ of the products did not yield a correlation as shown in the supplementary information (Fig S8). To check if the unequal

VMRs detected by INMS for each carbon source were responsible for the variations in average reaction affinities, the VMRs for all carbon sources were set to that of CO from Table 1 and affinities were calculated. The results are displayed in Fig 4 as orange dots that do not differ significantly from the average affinities for measured VMRs. Thus, the differences in detected VMRs are insufficient to explain the differences in reaction affinities among carbon sources.

Relatively oxidized carbon sources likely yield higher affinities when used in organic synthesis reactions because Enceladus's subsurface is a relatively reducing environment given the significant amount of H_2 (0.4-1.4%) detected in the plume gas by Cassini's INMS (Waite et al., 2017). This abundance of H_2 is rivaled only by a few hydrothermal vent systems on Earth, which are sources of known abiotic organic synthesis (McDermott et al., 2015). Coupled with the more oxidized carbon sources, H_2 is often a reactant, and its large aqueous activity combined with its high stoichiometries drives affinities to positive values (Eqn 4 & 5).

To explicitly explore how H_2 stoichiometry affects reaction affinities, the affinities of formation from each carbon source to all organic compounds, normalized per mole of carbon in the product, were plotted in Fig 5 as a function of H_2 stoichiometry in the reactions. This normalization was done to remove the effects of the size of each molecule on reaction affinity as is apparent in Fig 2. Again, only affinities calculated using aqueous activities calculated using the VMR from the median temperature of the tiger stripes (197 K) are shown. Negative stoichiometries indicate that H_2 is a reactant while positive stoichiometries indicate that H_2 is a product. One subplot was made for each carbon source, ordered from most oxidized on top (CO_2) to most reduced (CH_4). Each data point corresponds to the affinity calculated for the formation of an organic compound from one carbon source. Reaction affinities for each organic compound are displayed seven times – once per carbon source. Points are colored by $\bar{Z}_C$ of the product molecule.

One obvious feature from this perspective is the horizontal trends along H_2 stoichiometries from each carbon source. These horizontal trends converge towards the affinity value for compounds with an average oxidation state of carbon of -2. A $\bar{Z}_C$ of -2 is the value approached with continuous additions of CH_2 groups. Compounds in a series (C_1 to C_8 alkanes and alcohols, C_3 to C_8 ketones, C_3 to C_{10} aldehydes, and C_1 to C_{12} thiols and alkanoic acids) follow or converge along the horizontal trend, with the larger compounds in the series at the more extreme ends of H_2 stoichiometry. The magnitude of affinity, however, is determined by the carbon source and its stability within the modeled environment. The trend in Fig 4 can be observed in Fig 5, where reactions from HCN result in the highest affinities, followed by CO, CO_2, C_2H_2, C_3H_6, C_2H_6, and CH_4. Generally, but not perfectly, this hierarchy can be explained by the $\bar{Z}_C$ of the carbon source. Within subplots from each carbon source, a similar trend is apparent. It is consistently more favorable to produce reduced compounds versus oxidized compounds, similarly reported in Liu et al. (2024). Additionally, reactions with negative stoichiometries for H_2 tend to have more positive affinities and vice versa. The reaction which requires the most negative

stoichiometry of H_2 is n-octylbenzene formed from CO_2. The balanced reaction (R1) is given by

$$14\ CO_2 + 39\ H_2 = 1\ C_6H_5C_8H_{17}\ (\text{n-octylbenzene}) + 28\ H_2O \quad . \qquad (R1)$$

The high number of H_2 molecules required to reduce the carbon in CO_2 to n-octylbenzene is easily supplied in this environment, and pushes the formation reaction forward, lowering the energy of the system. In contrast, the reaction with the highest positive stoichiometry for H_2 is that from CH_4 to guanosine, given by

$$10\ CH_4 + 5\ H_2O + 5\ NH_3 = 1\ C_{10}H_{13}N_5O_5\ (\text{guanosine}) + 26\ H_2 \quad . \qquad (R2)$$

To oxidize CH_4 to guanosine, H_2O is required as a reactant, and abundant H_2 is produced. The high activity of H_2 in the system combined with its large positive stoichiometry contributes to a very unfavorable forward reaction, and large negative affinity. Overall, the more H_2 that is produced as a product, the more negative affinity becomes. From this perspective, the effect of stoichiometry of species in a reaction on affinity calculations can be understood. These results are similarly strongly affected by the activities of each species in the reaction. If another ocean world does not have the reducing environment we expect Enceladus to have, then perhaps reduced carbon sources would yield more positive affinities.

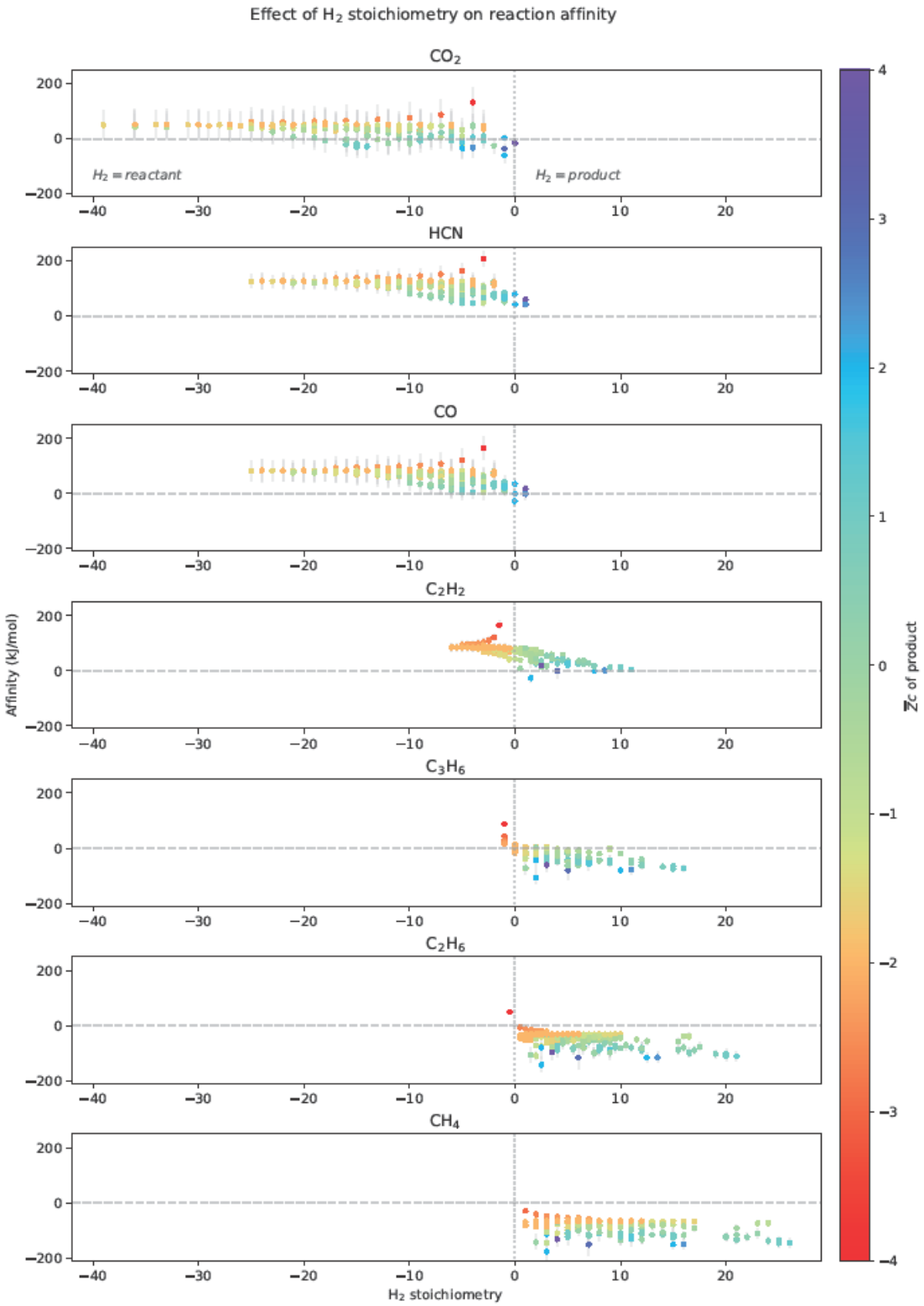

Figure 5. Affinities of reaction in kJ/mole for organic synthesis are normalized by moles of carbon in the product molecule and displayed as a function of H_2 stoichiometry in the reaction, where negative values indicate that H_2 is a reactant, and positive values indicate that H_2 is a product. Subplots are ordered by $\bar{Z}_C$ of the carbon source. Points are colored by the average oxidation state of carbon, $\bar{Z}_C$, of the product, where

purple is the most oxidized at +4 and red is the most reduced at -4. Horizontal dashed lines indicate equilibrium, or an affinity of 0 joules/mole of reaction. Vertical dotted lines indicate a stoichiometry of 0 for H_2.

Among all the components of an affinity calculation, it seems that the H_2 stoichiometry in each reaction most heavily affects the affinity results. This results from the large abundance of H_2 inferred for the ocean on Enceladus as indicated by the VMRs in the plumes, which causes more reduced compounds to be more thermodynamically stable and thus yield less energy when consumed for organic synthesis. Other ocean worlds are likely to yield different results. Let us explore what these results may mean for biosignature detection.

4.4 Distinguishing biosignatures from abiotic products

When a reaction has a positive affinity as written, energy would be released if the reaction were to proceed. Progress of the forward reaction will drive the system closer to equilibrium, and any resulting organic compounds would be *plausibly abiotic*. It may be possible that the reaction is actively progressing but has not yet reached equilibrium, perhaps due to kinetic barriers. Alternatively, a negative affinity would indicate that there is more product than is thermodynamically favorable. This means that the reverse reaction would release energy, while the forward reaction would require energy. If we are modeling the environment correctly in which the molecule was synthesized and an affinity calculation for the formation reaction in those conditions yielded a negative affinity, there must have been some kind of energy input for synthesis to occur. This could involve external energy input of an abiotic nature, such as surface impacts or radiation, or perhaps from the biological coupling of endergonic reactions with exergonic reactions. In living systems, the synthesis of biomolecules generally requires energy, but thanks to the complex machinery evolved over the history of life on Earth, energy-releasing chemical reactions are used to fuel energy-requiring anabolic processes. Chemotrophic life on Earth can harvest chemical energy from chemical reactions and store it in molecules like ATP. This stored energy is then used to build biomolecules. If there was a biosphere on Enceladus, it may have evolved similar mechanisms. Therefore, if we detect an organic molecule in an abundance that seems to be thermodynamically unstable in its environment, it would be *possibly biotic,* and we may want to target the locations these molecules were found for further investigation.

There are a couple of caveats to this sorting process that should be considered. As for the case in which a positive affinity is calculated for molecular synthesis, it is possible that this molecule was produced biotically. There are examples of biological synthesis on Earth that are energetically favorable (Shock and Canovas, 2010). In fact, abiotic organic synthesis may have been key to the emergence of life on Earth, and primitive organisms may have taken advantage of energy-releasing biosynthesis reactions. Additionally, perhaps the energy gradient was irrelevant to the organism performing the reaction, and it synthesized the molecule regardless of its environmental stability, if it has a sufficiently evolved metabolism to fuel that reaction. On the other hand,

there are cases in which a negative affinity may not be a biosignature, including the case in which a molecule was synthesized abiotically, and the reaction was thermodynamically favorable, but that molecule was then transported into an environment where it was unstable, and it has not been broken down yet. Likewise, the conditions around the molecule may have changed, causing it to become unstable with respect to its environment, and it has not yet been broken down. Investigations into icy moons pose the challenge of not having any spatial resolution. For Enceladus, we have the plume gas detected by Cassini, and it may well be an average of the conditions of the various potential sources of the plume. Additionally, impact of plume material onto the INMS likely caused degradation of source molecules and generation of byproducts, as modeled by Jaramillo-Botero et al. (2012). Until there is more spatial resolution, and the effects of impact velocities on detected molecules are better understood, there will be uncertainty about whether a molecule was produced in the conditions that we are modeling.

Using only CO_2 as a carbon source for organic synthesis on Enceladus results predominantly in positive affinities, with the exception of some oxidized compounds such as sugars and nucleobases (Fig S7). As in Liu et al. (2024), affinities for the synthesis of formaldehyde and acetylene from CO_2 are negative. However, there is no reason to assume such compounds originated from only CO_2. If we only consider CO_2 as a plausible carbon source, we may believe these compounds to be biosignatures. In contrast, with a full picture of potential carbon sources we conclude that formation of these molecules at the chosen abundance of 1 ppm would be thermodynamically favorable, and therefore *plausibly abiotic*. On Enceladus, it seems that there are favorable avenues for the synthesis of all compounds considered in this study, depending on the source of carbon used in the calculations. Therefore, volatile organics detected by INMS (Waite et al., 2009) and those mixed in with the ice grains measured by CDA (Khawaja et al., 2019) may not be most easily explained by the presence of life. However, reactions to form more complex molecules may require energy, especially if we allow the carbon to be consumed by organic synthesis, which was not done here. In these cases, it may become difficult to explain their presence without biological processes. Therefore, such compounds may be placed in the category *possibly biotic*. While they may be biotically produced, they are not required to be so.

5. CONCLUDING REMARKS

The results presented here demonstrate that reactions to form many aqueous organic compounds can be thermodynamically favorable with at least one of the carbon sources detected in the plumes on Enceladus. Therefore, if any of these hypothetical organic compounds were detected, the interpretation would be the same: these compounds are *plausibly abiotic*. The homogeny of these interpretations may seem lackluster, but as more complicated models are built, texture may emerge. For example, reactions could be written from detected precursors to more than one organic product per reaction, accounting for better mass balance between the carbon sources and a multitude of organic products. This would be a step in the right direction regarding the quantification

of energy required to make whole cells. Afterall, carbon sources may run out as more organic material is generated. The limited supply of each carbon source is not captured in this study. Additionally, biomolecules themselves can be much more massive and complicated. With increased abilities to estimate thermodynamic properties of organic molecules, we may one day be able to model the thermodynamic stability of more convincing biosignatures.

ACKNOWLEDGEMENTS

The authors would like to thank the Exploring Ocean Worlds NASA award 80NSSC19K1427 for partially funding these efforts, in addition to NASA FINESST award 80NSSC21K1539 for funding J. Robare's graduate research, and NASA SCoPE for funding J. Robare's travel to the American Geophysical Union Fall Meeting of 2023 to present an earlier version of this research. We also thank Vincent Milesi for a thorough review of this paper. J. Robare also thanks Dr. Grayson Boyer for his invaluable wisdom and guidance regarding thermodynamic calculations.

REFERENCES

Amend J.P., Helgeson H.C., 1997. Calculation of the standard molal thermodynamic properties of aqueous biomolecules at elevated temperatures and pressures. Part 1. l-α-amino acids. *J. Chem. Soc.*, Faraday Transactions 93(10): 1927–1941. https://doi.org/10.1039/A608126F

Anderson, G.M., 2005. *Thermodyn. Nat. Syst*. Cambridge University Press.

Barge, L.M. and Fournier, G.P., 2024. Considerations for detecting organic indicators of metabolism on Enceladus. *Astrobiol.*, 24(3), pp.328-338. https://doi.org/10.1089/ast.2023.0074

Boyer, G., 2021. pyCHNOSZ v0.7.0 (v0.7.0). Zenodo. https://doi.org/10.5281/zenodo.5539919

Burton, A.S. and Berger, E.L., 2018. Insights into abiotically-generated amino acid enantiomeric excesses found in meteorites. *Life*, 8(2), p.14. https://doi.org/10.3390/life8020014

Canovas P.A. III, Shock E.L. 2016. Geobiochemistry of metabolism: Standard state thermodynamic properties of the citric acid cycle. *Geochim. Cosmochim. Acta* 195: 293–322. https://doi.org/10.1016/j.gca.2016.08.028

Cronin, J.R., 1989. Origin of organic compounds in carbonaceous chondrites. *Adv. Sp. Res.*, 9(2), pp.59-64. https://doi.org/10.1016/0273-1177(89)90364-5

Cronin, J.R. and Pizzarello, S., 1983. Amino acids in meteorites. *Adv. Sp. Res.*, 3(9), pp.5-18. https://doi.org/10.1016/0273-1177(83)90036-4

Dale J.D., Shock E.L., MacLoed G., Aplin A.C., Larter S.R., 1997. Standard partial molal properties of aqueous alkylphenols at high pressures and temperatures. *Geochim. Cosmochim. Acta* 61(19): 4017–4024. https://doi.org/10.1016/S0016-7037(97)00212-3

De Sanctis, M.C., Ammannito, E., McSween, H.Y., Raponi, A., Marchi, S., Capaccioni, F., Capria, M.T., Carrozzo, F.G., Ciarniello, M., Fonte, S. and Formisano, M., 2017.

Localized aliphatic organic material on the surface of Ceres. *Sci.*, 355 (6326), pp.719-722. https://doi.org/10.1126/science.aaj2305

Dick, J.M., 2019. CHNOSZ: Thermodynamic calculations and diagrams for geochemistry. *Front. Earth Sci.*, 7, p.180. https://doi.org/10.3389/feart.2019.00180

Dick J.M., Evans K.A., Holman A.I., Jaraula C.M.B., Grice K., 2013. Estimation and application of the thermodynamic properties of aqueous phenanthrene and isomers of methylphenanthrene at high temperature. *Geochim. et Cosmochim. Acta* 122: 247–266. https://doi.org/10.1016/j.gca.2013.08.020

Dick, J.M. and Shock, E.L., 2011. Calculation of the relative chemical stabilities of proteins as a function of temperature and redox chemistry in a hot spring. *PLoS ONE* **6**(8), e22782. https://doi.org/10.1371/journal.pone.0022782

Dick, J. M., & Shock, E. L., 2021. The release of energy during protein synthesis at ultramafic-hosted submarine hydrothermal ecosystems. *J. Geophys. Res.* Biogeosciences, 126 (11), e2021JG006436. https://doi.org/10.1029/2021jg006436

Elsila, J.E., Aponte, J.C., Blackmond, D.G., Burton, A.S., Dworkin, J.P. and Glavin, D.P., 2016. Meteoritic amino acids: Diversity in compositions reflects parent body histories. *ACS Cent. Sci.*, 2(6), pp. 370-379. https://doi.org/10.1021/acscentsci.6b00074

Ensign, S.A., Hyman, M.R. and Arp, D.J., 1992. Cometabolic degradation of chlorinated alkenes by alkene monooxygenase in a propylene-grown Xanthobacter strain. *Appl. and Environ. Microbiol.*, 58(9), pp. 3038-3046. https://doi.org/10.1128/aem.58.9.3038-3046.1992

Epstein, S., Krishnamurthy, R.V., Cronin, J.R., Pizzarello, S. and Yuen, G.U., 1987. Unusual stable isotope ratios in amino acid and carboxylic acid extracts from the Murchison meteorite. *Nat.*, 326 (6112), pp. 477-479. https://doi.org/10.1038/326477a0

Freissinet, C., Glavin, D.P., Mahaffy, P.R., Miller, K.E., Eigenbrode, J.L., Summons, R.E., Brunner, A.E., Buch, A., Szopa, C., Archer Jr, P.D. and Franz, H.B., 2015. Organic molecules in the Sheepbed mudstone, Gale crater, Mars. *J. Geophys. Res. Planets*, 120(3), pp. 495-514. https://doi.org/10.1002/2014JE004737

Glein, C.R., Baross, J.A. and Waite Jr, J.H., 2015. The pH of Enceladus' ocean. *Geochim. et Cosmochim. Acta*, 162, pp. 202-219. https://doi.org/10.1016/j.gca.2015.04.017

Glein, C.R., Postberg, F. and Vance, S.D., 2018. The geochemistry of Enceladus: Composition and controls. *Enceladus and the Icy Moons of Saturn*, P. M. Schenk, R. N. Clark, C. J. A. Howett, A. J. Verbiscer, J. H. Waite, Eds. University of Arizona Press, Tucson, pp. 39-56.

Glein, C. R., & Waite, J. H., 2020. The carbonate geochemistry of Enceladus' ocean. *Geophys. Res. Lett.*, 47, e2019GL085885. https://doi.org/10.1029/2019GL085885

Goguen, J.D., Buratti, B.J., Brown, R.H., Clark, R.N., Nicholson, P.D., Hedman, M.M., Howell, R.R., Sotin, C., Cruikshank, D.P., Baines, K.H. and Lawrence, K.J., 2013. The temperature and width of an active fissure on Enceladus measured with Cassini VIMS during the 14 April 2012 South Pole flyover. *Icarus*, 226 (1), pp.1128-1137. https://doi.org/10.1016/j.icarus.2013.07.012

638 Hahn, C.J., Lemaire, O.N., Kahnt, J., Engilberge, S., Wegener, G. and Wagner, T., 2021.
639 Crystal structure of a key enzyme for anaerobic ethane activation. *Sci.*, 373 (6550),
640 pp.118-121. https://doi.org/10.1126/science.abg1765
641 Hawrylak B., Palepu R., Tremaine P.R.. 2006. Thermodynamics of aqueous
642 methyldiethanolamine (MDEA) and methyldiethanolammonium chloride
643 (MDEAH+Cl−) over a wide range of temperature and pressure: Apparent molar
644 volumes, heat capacities, and isothermal compressibilities. *J. Chem. Thermodyn.*
645 38(8): 988–1007. https://doi.org/10.1016/j.jct.2005.10.013
646 Haynes, W. M., 2014. *CRC Hand. Chem. Phys.* (Internet Version 2014), 94th ed. CRC
647 Press/Taylor and Francis, Boca Raton, FL. https://doi.org/10.1201/9781315380476
648 Jaramillo-Botero, A., An, Q., Cheng, M.J., Goddard III, W.A., Beegle, L.W. and Hodyss,
649 R., 2012. Hypervelocity Impact Effect of Molecules from Enceladus' Plume and Titan's
650 Upper Atmosphere on NASA's Cassini Spectrometer from Reactive Dynamics
651 Simulation. *Phys. Rev. Let.*, 109 (21), p.213201.
652 Khawaja, N., Postberg, F., Hillier, J., Klenner, F., Kempf, S., Nölle, L., Reviol, R., Zou, Z.
653 and Srama, R., 2019. Low-mass nitrogen-, oxygen-bearing, and aromatic compounds
654 in Enceladean ice grains. *Mon. Not. Royal Astronomical Soc.*, 489 (4), pp.5231-5243.
655 King, G.M. and Weber, C.F., 2007. Distribution, diversity and ecology of aerobic CO-
656 oxidizing bacteria. *Nat. Rev. Microbiol.*, 5 (2), pp.107-118.
657 https://doi.org/10.1038/nrmicro1595
658 Kitadai N., 2014. Thermodynamic prediction of glycine polymerization as a function of
659 temperature and pH consistent with experimentally obtained results. *J. Mol. Evol.*
660 78(3-4): 171–187. https://doi.org/10.1007/s00239-014-9616-1
661 Klenner, F., Postberg, F., Hillier, J., Khawaja, N., Cable, M.L., Abel, B., Kempf, S., Glein,
662 C.R., Lunine, J.I., Hodyss, R. and Reviol, R., 2020. Discriminating Abiotic and Biotic
663 Fingerprints of Amino Acids and Fatty Acids in Ice Grains Relevant to Ocean Worlds.
664 *Astrobiol.*, 20(10), pp.1168-1184.
665 Koga, T. and Naraoka, H., 2017. A new family of extraterrestrial amino acids in the
666 Murchison meteorite. *Sci. Rep.*, 7(1), p.636. https://doi.org/10.1038/s41598-017-
667 00693-9
668 LaRowe D.E., Amend J.P., 2019. The energetics of fermentation in natural settings.
669 *Geomicrobiol. J.* 36(6): 492–505. https://doi.org/10.1080/01490451.2019.1573278
670 LaRowe D.E., Amend J.P., 2016. The energetics of anabolism in natural settings. *The*
671 *ISME J*. 10(6): 1285–1295. https://doi.org/10.1038/ismej.2015.227
672 LaRowe D.E., Dick J.M., 2012. Calculation of the standard molal thermodynamic
673 properties of crystalline peptides. *Geochim. et Cosmochim. Acta* 80: 70–91.
674 https://doi.org/10.1016/j.gca.2011.11.041
675 LaRowe D.E., Helgeson H.C., 2006. Biomolecules in hydrothermal systems: Calculation
676 of the standard molal thermodynamic properties of nucleic-acid bases, nucleosides,
677 and nucleotides at elevated temperatures and pressures. *Geochim. et Cosmochim.*
678 *Acta* 70(18): 4680–4724. https://doi.org/10.1016/j.gca.2006.04.010

Liu, C., Xu, W., Zhang, Z., Robinson, K., Lau, M., Huang, F., Glein, C.R. and Hao, J., 2024. The Potential for Organic Synthesis in the Ocean of Enceladus. The *Astrophys. J.*, 971 (1), p.51.

Magee, B.A. and Waite, J.H., 2017, March. Neutral gas composition of Enceladus' plume-model parameter insights from Cassini-INMS. *48th Annual LPSC*. (No. 1964, p. 2974).

Marshall, S.M., Mathis, C., Carrick, E., Keenan, G., Cooper, G.J., Graham, H., Craven, M., Gromski, P.S., Moore, D.G., Walker, S.I. and Cronin, L., 2021. Identifying molecules as biosignatures with assembly theory and mass spectrometry. *Nat. Commun.*, 12(1), p. 3033. https://doi.org/10.1038/s41467-021-23258-x

Martins, Z., Botta, O., Fogel, M.L., Sephton, M.A., Glavin, D.P., Watson, J.S., Dworkin, J.P., Schwartz, A.W. and Ehrenfreund, P., 2008. Extraterrestrial nucleobases in the Murchison meteorite. *Earth and Planet. Sci. Lett.*, 270(1-2), pp.130-136. https://doi.org/10.1016/j.epsl.2008.03.026

McDermott, J.M., Seewald, J.S., German, C.R. and Sylva, S.P., 2015. Pathways for abiotic organic synthesis at submarine hydrothermal fields. *Proc. Natl. Acad. Sci.,* 112(25), pp.7668-7672. https://doi.org/10.1073/pnas.1506295112

McKay, C.P., Anbar, A.D., Porco, C. and Tsou, P., 2014. Follow the plume: the habitability of Enceladus. *Astrobiol.*, 14(4), pp.352-355. https://doi.org/10.1089/ast.2014.1158

Mumma, M.J. and Charnley, S.B., 2011. The chemical composition of comets—emerging taxonomies and natal heritage. *Annual Rev. of Astron. and Astrophys.*, 49, pp.471-524. https://doi.org/10.1146/annurev-astro-081309-130811

Neveu, M., Hays, L.E., Voytek, M.A., New, M.H. and Schulte, M.D., 2018. The ladder of life detection. *Astrobiol.*, 18(11), pp.1375-1402. https://doi.org/10.1089/ast.2017.1773

Neveu, M., Aspin, A., Naseem, M. and Yang, Z., 2024. Effect of the liquid-vacuum transition on the relative abundances of amino and fatty acids sought as biosignatures on icy ocean worlds. *Earth and Planet. Sci. Lett.*, 630, p.118622. https://doi.org/10.1016/j.epsl.2024.118622

Nguyen, A.N., Clemett, S.J., Thomas-Keprta, K., Keller, L.P., Glavin, D.P., Dworkin, J.P., Barnes, J.J., Zega, T.J., McCoy, T.J., Thompson, M.S. and Haenecour, P., 2024. Coordinated analysis of isotopically anomalous nanoglobules and insoluble organic matter in quick-look samples from asteroid Bennu. (abstract) *55th Lunar and Planet. Sci. Conf.*

Peter, J.S., Nordheim, T.A. and Hand, K.P., 2024. Detection of HCN and diverse redox chemistry in the plume of Enceladus. *Nat. Astronom.*, 8(2), pp.164-173. https://doi.org/10.1038/s41550-023-02160-0

Plyasunov A.V., Shock E. L., 2001. Correlation strategy for determining the parameters of the revised Helgeson-Kirkham-Flowers model for aqueous nonelectrolytes. *Geochim. et Cosmochim. Acta* 65(21): 3879–3900. https://doi.org/10.1016/S0016-7037(01)00678-0

Porco, C.C., Helfenstein, P., Thomas, P.C., Ingersoll, A.P., Wisdom, J., West, R., Neukum, G., Denk, T., Wagner, R., Roatsch, T. and Kieffer, S., 2006. Cassini observes the active south pole of Enceladus. *Sci.*, 311 (5766), pp.1393-1401. https://doi.org/10.1126/science.1123013

Postberg, F., Khawaja, N., Abel, B., Choblet, G., Glein, C.R., Gudipati, M.S., Henderson, B.L., Hsu, H.W., Kempf, S., Klenner, F. and Moragas-Klostermeyer, G., 2018. Macromolecular organic compounds from the depths of Enceladus. *Nat.*, 558 (7711), pp.564-568.

Postberg, F., Kempf, S., Hillier, J.K., Srama, R., Green, S.F., McBride, N. and Grün, E., 2008. The E-ring in the vicinity of Enceladus: II. Probing the moon's interior—the composition of E-ring particles. *Icarus*, 193 (2), pp.438-454.

Postberg, F., Kempf, S., Schmidt, J., Brilliantov, N., Beinsen, A., Abel, B., Buck, U. and Srama, R., 2009. Sodium salts in E-ring ice grains from an ocean below the surface of Enceladus. *Nat.*, 459 (7250), pp.1098-1101. https://doi.org/10.1038/nature08046

Postberg, F., Sekine, Y., Klenner, F., Glein, C.R., Zou, Z., Abel, B., Furuya, K., Hillier, J.K., Khawaja, N., Kempf, S. and Noelle, L., 2023. Detection of phosphates originating from Enceladus's ocean. *Nat.*, 618 (7965), pp.489-493. https://doi.org/10.1038/s41586-023-05987-9

Rosner, B.M., Rainey, F.A., Kroppenstedt, R.M. and Schink, B., 1997. Acetylene degradation by new isolates of aerobic bacteria and comparison of acetylene hydratase enzymes. *FEMS Microbiol. Lett.*, 148 (2), pp.175-180. https://doi.org/10.1111/j.1574-6968.1997.tb10285.x

Schulte M.D., 2010. Organic sulfides in hydrothermal solution: Standard partial molal properties and role in organic geochemistry of hydrothermal environments. *Aquat. Geochem.* 16(4): 621–637. https://doi.org/10.1007/s10498-010-9102-3

Schulte M.D., Rogers K.L., 2004. Thiols in hydrothermal solution: Standard partial molal properties and their role in the organic geochemistry of hydrothermal environments. *Geochim. et Cosmochim. Acta* 68(5): 1087–1097. https://doi.org/10.1016/j.gca.2003.06.001

Schulte M.D., Shock E.L., 1993. Aldehydes in hydrothermal solution: Standard partial molal thermodynamic properties and relative stabilities at high temperatures and pressures. *Geochim. et Cosmochim. Acta* 57(16): 3835–3846. https://doi.org/10.1016/0016-7037(93)90337-V

Sherwood Lollar, B., Atreya, S.K., Boss, A.P., Falkowski, P.G., Farmer, J.D., Guyon, O., Joyce, G.F., Kasting, J.F., Meadows, V.S., Neches, P.M., Pilcher, C.B., Renno, N.O., Rogers, K.L., Schmidt, B.E., Summons, R., Westall, F., Wright, S.A., 2018. *An Astrobiol. Strateg. for the Search for Life in the Univers*. National Academies of Sciences, Engineering, and Medicine, National Academy Press, Washington, DC.

Shock E.L., 1993. Hydrothermal dehydration of aqueous organic compounds. *Geochim. et Cosmochim. Acta* 57(14): 3341–3349. https://doi.org/10.1016/0016-7037(93)90542-5

Shock E.L., 1995. Organic acids in hydrothermal solutions: Standard molal thermodynamic properties of carboxylic acids and estimates of dissociation constants at high temperatures and pressures. *Am. J. Sci.* 295(5): 496–580. https://doi.org/10.2475/ajs.295.5.496

Shock, E., Canovas, P., 2010. The potential for abiotic organic synthesis and biosynthesis at seafloor hydrothermal systems. *Geofluids*, 10(1-2): 161-192.

765 Shock E.L., Helgeson H.C., 1990. Calculation of the thermodynamic and transport
766 properties of aqueous species at high pressures and temperatures: Standard partial
767 molal properties of organic species. *Geochim. et Cosmochim. Acta* 54(4): 915–945.
768 https://doi.org/10.1016/0016-7037(90)90429-O
769 Shock E.L., Koretsky C.M., 1993. Metal-organic complexes in geochemical processes:
770 Calculation of standard partial molal thermodynamic properties of aqueous acetate
771 complexes at high pressures and temperatures. *Geochim. et Cosmochim. Acta*
772 57(20): 4899–4922. https://doi.org/10.1016/0016-7037(93)90128-J
773 Shock E.L., McKinnon W.B., 1993. Hydrothermal processing of cometary volatiles—
774 Applications to Triton. *Icarus* 106(2): 464–477. https://doi.org/10.1006/icar.1993.1185
775 Shock, E.L. and Schulte, M.D., 1990. Amino-acid synthesis in carbonaceous meteorites
776 by aqueous alteration of polycyclic aromatic hydrocarbons. *Nat.*, 343(6260), pp.728-
777 731. https://doi.org/10.1038/343728a0
778 Waite, J.H., Glein, C.R., Perryman, R.S., Teolis, B.D., Magee, B.A., Miller, G., Grimes, J.,
779 Perry, M.E., Miller, K.E., Bouquet, A. and Lunine, J.I., 2017. Cassini finds molecular
780 hydrogen in the Enceladus plume: Evidence for hydrothermal processes. *Sci.*,
781 356(6334), pp.155-159. https://doi.org/10.1126/science.aai8703
782 Waite, J.H., Lewis, W.S., Kasprzak, W.T., Anicich, V.G., Block, B.P., Cravens, T.E.,
783 Fletcher, G.G., Ip, W.H., Luhmann, J.G., McNutt, R.L. and Niemann, H.B., 2004. The
784 Cassini ion and neutral mass spectrometer (INMS) investigation. *Space Sci. Rev*. 114,
785 113–231 (2004). https://doi.org/10.1007/978-1-4020-2774-1_2
786 Waite Jr, J.H., Lewis, W.S., Magee, B.A., Lunine, J.I., McKinnon, W.B., Glein, C.R.,
787 Mousis, O., Young, D.T., Brockwell, T., Westlake, J. and Nguyen, M.J., 2009. Liquid
788 water on Enceladus from observations of ammonia and ^{40}Ar in the plume. *Nat.*,
789 460(7254), pp.487-490. https://doi.org/10.1038/nature08153
790 Yanez, M.D., LaRowe, D.E., Cable, M.L. and Amend, J.P., 2024. Energy yields for
791 acetylenotrophy on Enceladus and Titan. *Icarus*, p.115969.
792 https://doi.org/10.1016/j.icarus.2024.115969